JOURNAL OF SOLID STATE CHEMISTRY 93, 283–290 (1991)

Kinetics of the Reduction of Fe_2O_3 with Hydrogen

MAHMOUD M. KHADER, BAHGAT E. EL-ANADOULI, EMAD EL-NAGAR, AND BADR G. ATEYA

Chemistry Department, Faculty of Science, Cario University, Cairo, Egypt

Received October 10, 1990; in revised form March 4, 1991

The kinetics of the heterogeneous reduction of Fe_2O_3 with gaseous hydrogen was studied over the temperature range of 300–400°C. As Fe_2O_3 is reduced, the resulting oxygen vacancies act as anion dopants of the remaining Fe_2O_3, thus increasing its conductivity. The final reaction product is FeO. It reoxidizes quickly upon exposure to air forming Fe_3O_4, as revealed by X-ray diffraction analysis. The progress of the reaction was followed by measuring the variation of the electrical conductivity of sintered compressed pellets with time. The variation of conductivity with the time of reduction was found to be quite complex, and can be divided into three regions: (a) region I, at short times, where the process is controlled by the chemical reaction at the outer surface between hydrogen and ferric oxide. This is an activated reaction characterized by an activation energy of 56.5 kJ $mole^{-1}$; (b) region II, which signals the onset of diffusion control on the overall rate of the process, where the reaction starts to penetrate through the solid phase. Within this region, it was found that the conductivity varied linearly with the square root of the time; and (c) region III where the process is controlled by diffusion through the solid phase. The behavior of the system in regions II and III was found to be in agreement with the predictions obtained from solving Fick's second law of diffusion.

1. Introduction

The reduction of ferric oxide with hydrogen has always been a subject of considerable interest for the steel industry (*1–3*) and more recently in connection with photoelectrochemistry (*4–8*). The presence of some Fe(II) species within the ferric oxide corundum lattice increased its photoconductivity considerably (*4, 8*). Gardner *et al.* (*9*) showed that conduction in ferric oxide was due to the presence of either foreign impurities or oxygen vacancies. They reported that molecular oxygen loss, leading to the formation of metal excess, occurred upon firing the stoichiometric ferric oxide in air above 1000°C. However, below about 1000°C, no oxygen loss was detected. The stability of Fe(II) species on the surface of single crystals of Fe_2O_3 was studied by Hendewerk *et al.* (*10*) at different temperatures and low pressures of water vapor. These workers concluded that Fe(II) could only exist in the subsurface region underneath a layer of Fe_2O_3,

The purpose of the present paper is to study the kinetics of reduction of ferric oxide with hydrogen. Electrical conductivity measurements *in situ* were used for this purpose.

2. Experimental Details

2.1. Sample Preparation

Ferric oxide powder (α-products 99.99%) was compressed in the form of pellets at a pressure of 10 tons per square centimeter. The pellets had a diameter of 1.3 cm and

0022-4596/91 $3.00

thicknesses from 0.05 to 0.12 cm. They were sintered in air at 1000°C for 24 hr, and then cooled in air to room temperature. The sintering process was accompanied with considerable reduction in volume and increase in density, grain size, and hardness and practically negligible weight loss (0.6%). The density of the sintered Fe_2O_3 pellets was 5.187 g cm^{-3} as compared to a true density of 5.24 g cm^{-3}, thus corresponding to a volume porosity of about 1%. The weight loss upon sintering was only a fraction of 1%, indicating no significant change in the stoichiometry or the phase structure.

2.2. *Electrical Conductivity Measurements*

The conductivity cell was composed of two platinum foil electrodes of 1.5 cm diameter. Each electrode was sealed tightly to a steel disk of about an equal diameter. One of the two steel disks was fixed to the frame of the cell holder while the other could be pressed with the aid of a spring against the former.

Electrical leads were spot-welded to both electrodes, and a chromel–Alumel thermocouple was kept in contact with one of the electrodes. The sample was coated with a silver paint (in a volatile solvent) which deposits a thin layer of silver powder on its surface. The sample was positioned between the two electrodes and held tightly with the spring.

The cell holder was positioned in a horizontal tube furnace on cold and heating was started. After the temperature stabilized, a stream of hydrogen gas was allowed to flow past the pellet. Two water bubblers were positioned at both ends of the furnace.

The electrical conductivity was measured by an EG & G Princeton Applied Research Model 363 electrometer using the current–voltage technique. The electrical power on the sample was limited to 0.1 W per cubic centimeter to prevent excessive joule heating.

2.3. *Reduction of Ferric Oxide*

Electrical conductivity measurements were followed during the reduction of ferric oxide pellets. The reduction was performed at different temperatures for various periods of time. In each case a fresh pellet was used.

2.4. *X-Ray Diffraction Analysis*

X-ray diffraction analysis of the pellets was made by using a Siemens Model D500 diffractometer equipped with a copper $K\alpha$ radiation source. Measurements were undertaken in the range of from $2\theta = 15°$ to 65°. The grain width in the sintered pellets was estimated to be about 30–50 μm as revealed by scanning electron microscopy.

3. Results and Discussion

3.1. *Effect of H_2 Reduction on the Conductivity of Fe_2O_3*

Figure 1 represents the conductivity, σ, versus the time of reduction for Fe_2O_3 pellets of different thicknesses. The significant increase in the conductivity upon reduction is attributed to doping of the Fe_2O_3 corundum lattice by Fe(II). The weight loss upon reduction indicates that the final product is FeO. It reoxidizes quickly upon exposure to air to form Fe_3O_4, which was confirmed by weight gain and X-ray powder diffraction analysis. Figure 2 shows the X-ray diffraction patterns of (a) Fe_2O_3 and (b) the reduction product after exposure to air (the reduction was performed for 1 hr at 400°C). The diffraction pattern in (b) is identical to that of Fe_3O_4. Note the complete disappearance of the largest peak of Fe_2O_3 (at $2\theta = 33.2°$) in the pattern of the reduced sample.

We can attempt to explain such an increase in the conductivity due to the formation of Fe(II) in light of the solid state band model of semiconductors. In this model, the band-energy diagram of ferric oxide, as proposed by Goodenough (*11*), shows that the valence band is formed mainly from the oxy-

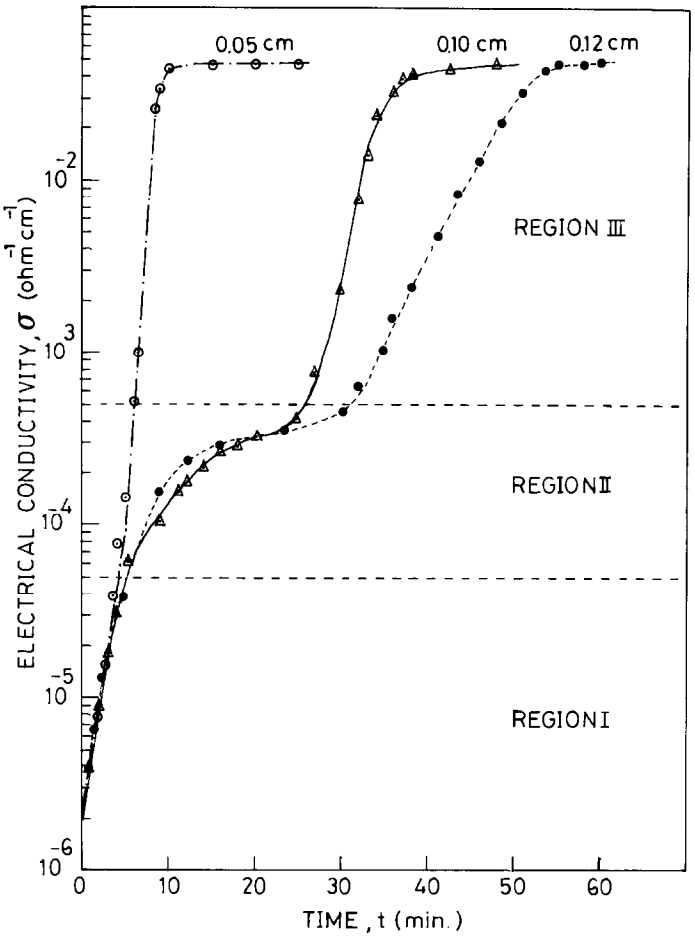

FIG. 1. Variation of the electrical conductivity σ with time at 400°C for three pellets of the same area (1.3 cm^2) and thicknesses of 0.12 (●), 0.1 (△) and 0.05 cm (⊙).

gen : $2p$ and a small contribution from the Fe : $3d$ atomic orbitals. During the reduction step oxygen vacancies are formed according to the reaction

$$\text{Fe(III): } O + H_2 \rightarrow \text{Fe(II)} - V_a^{\cdot\cdot} + H_2O, \quad (1)$$

where $V_a^{\cdot\cdot}$ refers to the oxygen (anion) vacancy. Since the Fe(II) species (or the oxygen vacancies) are impregnated in the Fe_2O_3 lattice, the extra electron on the Fe(II) will have no valence orbital to occupy; consequently, it must exist within the forbidden region of the remaining Fe_2O_3. In this sense, the oxygen vacancies, formed by the H_2 reduction, act like anion dopants for Fe_2O_3, and their energies must be near to the bottom edge of the conduction band of Fe_2O_3.

The increase in the conductivity is due to an increase in the carrier concentration. Both quantites are related by the equation,

$$\sigma = en\mu_i, \quad (2)$$

where e is the electronic charge, μ_i is the i-

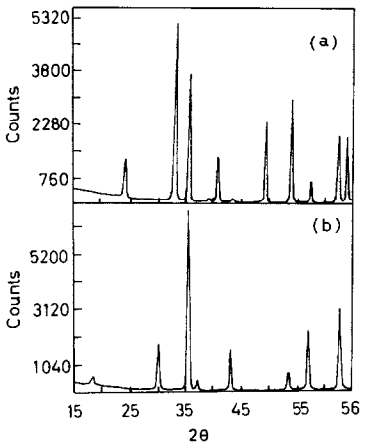

FIG. 2. X-ray diffraction patterns of (a) Fe_2O_3 before reduction and (b) the reduction product after exposure to air.

carrier mobility, and n is the carrier concentration.

From Eqs. (1) and (2), the conductivity increases with time as does the rate of generation of oxygen vacancies. The mode of variation of conductivity with time can be divided into three regions, as shown in Fig. 1.

Region I occurs at short times, during which the conductivity increases rather quickly with time. The rate of increase is practically independent of the thickness of the pellet, although it depends on the temperature (cf. Fig. 3). This indicates that, in this region, the process is controlled by the chemical reaction occurring at the surface of the pellet.

Region II occurs at intermediate times. This is a transition region during which the conductivity depends on both the time of reduction and the thickness of the pellet.

Region III occurs at long times. During this region, the conductivity is significantly affected by the thickness of the pellet. It increases with time, reaching a limiting value at long times. This limiting value is independent of the thickness of the pellet. However, it is quite clear that the time needed to approach this limiting value depends on the thickness of the pellet.

It is quite evident that while region I is controlled by the rate of the chemical reaction occurring at the surface of the pellet (i.e., without diffusion limitation), regions II and III describe the behavior of the system under moderate and strong diffusion control, respectively. These regions are analyzed below in more detail.

Region I. The chemical reaction occurring at the pellet surface may be represented by

$$Fe_2O_3 + H_2 \rightarrow 2\ FeO[V_a^-] + H_2O \quad (3)$$

Equation (3) is equivalent to Eq. (1). As more FeO is produced, more oxygen vacancies are generated. Consequently, the conductivity increases with time. The weight loss observed upon reduction corresponds closely to Eq. (3). However, some of the resulting FeO reoxidizes upon exposure to air, back to Fe_2O_3. The final product is Fe_3O_4, which forms as

$$2\ FeO[V_a^-] + 2\ Fe_2O_3 \rightarrow 2\ Fe_3O_4[V_a^-]. \quad (4)$$

The presence of Fe_3O_4 as a product of Eq. (4) has been confirmed by weight gain upon

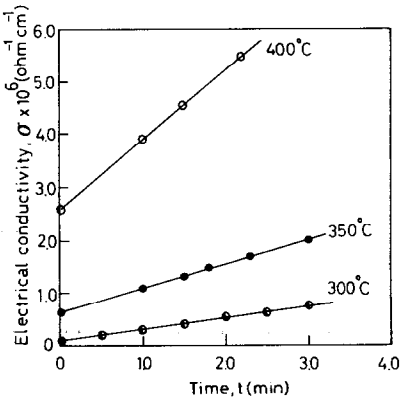

FIG. 3. The relation between ln σ and time of reduction for pellets of the same dimensions at 300 (◐), 350 (●), and 400°C (○).

exposure of the reduced powder to air and by X-ray powder diffraction measurements, see Fig. 2. The above reaction scheme appears to be quite complicated. However, for the purpose of this study, one can determine a reaction rate constant using the method of initial rates (*12*), i.e., from the slope of a plot of σ versus t, at short times. Note that σ_t is proportional to the number of charge carriers (i.e., the number of oxygen vacancies) at time t. Figure 3 shows such plots for pellets of thickness 0.1 cm at temperatures of 300, 350, and 400°C.

The rate of the reaction is the rate of generation of vacancies per second, i.e.,

$$dn/dt = k[Fe_2O_3]P_{H_2}, \qquad (5)$$

where k is the standard rate constant of the reaction, $[Fe_2O_3]$ is the concentration of the Fe_2O_3, and P_{H_2} is the partial pressure of the hydrogen gas. The concentration of ferric oxide will be taken in mole fractions, i.e., unity and the partial pressure of hydrogen is assumed unity. Furthermore, by virtue of Eq. (2),

$$dn/dt = \frac{1}{\mu e} d\sigma/dt; \qquad (6)$$

thus the standard rate constant, k, of the reaction is given by

$$k = \frac{1}{\mu e} d\sigma/dt. \qquad (7)$$

It is to be understood that the rate constant pertains to a unit mole fraction of Fe_2O_3 and 1 atm of H_2 gas. The value of the carrier mobility can be estimated from the limiting value of σ represented in Fig. 1, and the principles of chemical calculations as applied to Eqs. (3) and (4). The value of carrier mobility μ comes out to be 5.5×10^{-5} cm^2 sec^{-1} V^{-1} at 400°C.

The standard rate constants, calculated from Fig. 3, are 6.75×10^{-10}, 1.48×10^{-9}, and 4.32×10^{-9} atm^{-1} sec^{-1} at 300, 350, and 400°C, respectively. It is clear that as the temperature increases, the standard rate constant of the process increases; i.e., the reduction process is activated. For such processes, the rate constant is given by the Arrhenius equation,

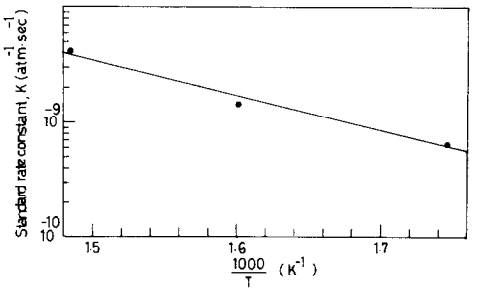

FIG. 4. The logarithm of the standard rate constant $k(T)$ (from the slopes of Fig. 3) versus $1/T$.

$$\ln k(T) = -\frac{E}{RT} + \text{constant}, \qquad (8)$$

where E is the activation energy, R is the gas constant, and T is the absolute temperature. Thus a plot of ln $k(T)$ versus $1/T$ gives a straight line from the slope of which the activation energy can be calculated. This is shown in Fig. 4, which is quite a satisfactory straight line. The activation energy of the process comes out to be 56.5 kJ mole^{-1} which is in good agreement with the value reported by McKewan (*13*).

Regions II and III. The transport of hydrogen through the pellet can be analyzed through the solution of the diffusivity equation. For the diffusion of hydrogen through the pellet, Fick's second law states that

$$\frac{\partial C(x, t)}{\partial t} = D\frac{\partial^2 C(x, t)}{\partial x^2}, \qquad (9)$$

where $C(x, t)$ is the concentration of hydrogen at a distance x and time t within the pellet, and D is the diffusion coefficient, which is assumed to be constant.

Figure 5 is a schematic of the physical picture illustrating the coordinates and time effects on the process. The pellet is initially

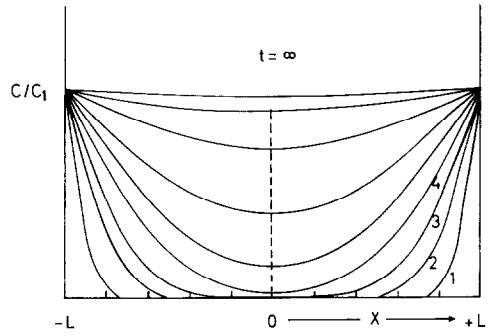

FIG. 5. Schematic representation of the physical picture of the system and the evolution of the diffusion process. Curves 1, 2, 3, etc., represent increasing time of reduction.

free from any hydrogen. Its outer surface is exposed to a stream of H_2 gas, which maintains the concentration of hydrogen constant at the outer surface of the pellet. This physical picture corresponds to the following boundary conditions:

$$t = 0, \quad C(x, o) = 0, \quad -L < x < +L \tag{10}$$

$$t > 0, \quad C(o, t) = C_1$$

The solution of Eq. (9) with these boundary conditions is given by (*14*)

$$\frac{C}{C_1} = 1 - \frac{4}{\pi}\sum_{n=0}^{n=\infty}\frac{(-1)^n}{2n+1} \times \exp[-(2n+1)^2\pi^2 Dt/4L^2] \times \cos\frac{(2n+1)\pi x}{2L}, \tag{11}$$

where L is half the thickness of the pellet. In our work, the thickness of the pellet was small enough compared to its diameter to ensure negligible edge effects. This becomes true if the ratio of thickness : diameter is ≤ 0.1 (*14*).

The total amount of hydrogen which had diffused into both faces of the pellet after time t, M_t, is related to the saturation value, M_∞, by

$$\frac{M_t}{M_\infty} = 1 - \sum_{n=0}^{n=\infty}\frac{8}{(2n+1)^2\pi^2} \times \exp[-(2n+1)^2\pi^2 Dt/4L^2]. \tag{12}$$

Since M and σ are both proportional to the number of charge carriers (oxygen vacancies), it follows that

$$\frac{M_t}{M_\infty} = \frac{\sigma_t}{\sigma_\infty}. \tag{13}$$

The above solutions converge to simpler equations at short times, i.e.,

$$\frac{C}{C_1} = \sum_{n=0}^{n=\infty}(-1)^n \operatorname{erfc}\frac{(2n+1)(L-x)}{2\sqrt{Dt}} + \sum_{n=0}^{n=\infty}(-1)^n \operatorname{erfc}\frac{(2n+1)(L+x)}{2\sqrt{Dt}} \tag{14}$$

$$\frac{\sigma_t}{\sigma\infty} = 2\frac{\sqrt{Dt}}{L}\left[\frac{1}{\sqrt{\pi}} + 2\sum_{n=1}^{n=\infty}(-1)^n \operatorname{ierfc}\frac{nL}{\sqrt{Dt}}\right] \tag{15}$$

$$\text{as } t \to 0, \frac{nL}{\sqrt{Dt}} \to \infty; \operatorname{ierfc}\frac{nL}{\sqrt{Dt}} \to 0.$$

Thus

$$\frac{\sigma_t}{\sigma_\infty} = 2\sqrt{\frac{Dt}{\pi L}}, \tag{16}$$

where σ_t is the conductivity of the reduced sample at time t and σ_∞ is the conductivity of the fully reduced material. The latter corresponds to the conductivity of FeO.

3.2. Beginning of the Diffusion Regime

Equation (16) represents the beginning of the diffusion regime, region II in Fig. 1. From Eq. (16), a plot of σ_t/σ_∞ versus $\sqrt{t}$ gives a straight line with a slope of $(2/L)\sqrt{D/\pi}$; i.e., the slope is inversely proportional to half of the thickness.

The data in region II of Fig. 1 do indeed obey Eq. (16) for the three thicknesses; i.e.,

TABLE I

VALUES OF $t_{(x)}/L^2$ FOR PELLETS OF DIFFERENT THICKNESSES AT THREE VALUES OF σ_t/σ_∞ (THE DATA ARE TAKEN FROM FIG. 1)

	σ_t/σ_∞		
L (cm)	1/4	1/2	3/4
0.025	$1.20 \pm 0.08 \times 10^4$	$1.28 \pm 0.08 \times 10^4$	$1.44 \pm 0.08 \times 10^4$
0.050	$1.28 \pm 0.02 \times 10^4$	$1.36 \pm 0.02 \times 10^4$	$1.44 \pm 0.02 \times 10^4$
0.060	$1.26 \pm 0.01 \times 10^4$	$1.36 \pm 0.01 \times 10^4$	$1.41 \pm 0.01 \times 10^4$

they give straight line plots between σ_t/σ_∞ and $\sqrt{t}$. Furthermore, the slopes are inversely proportional to half the thickness of the pellet, as Fig. 6 reveals. This confirms that region II in Fig. 1 signals the onset of diffusion control of the process.

The diffusion coefficient of hydrogen through the Fe_2O_3 pellet can be evaluated from the slope of the straight line plot of Fig. 6, which is equal to $2\sqrt{D/\pi}$. From this set of data, the diffusion coefficient comes out to be 2.8×10^{-10} cm^2 sec^{-1} at 400°C.

Equation (12) describes the general behavior under diffusion control. The short time limit was analyzed above. At longer times, the equation predicts that M_t/M_∞ increases with time rather nonlinearly and approaches unity at longer times. A full analysis of the diffusion problem is beyond the scope of this paper. It will suffice here to prove that region III corresponds to diffusion control, as given by Eq. (12) at long times.

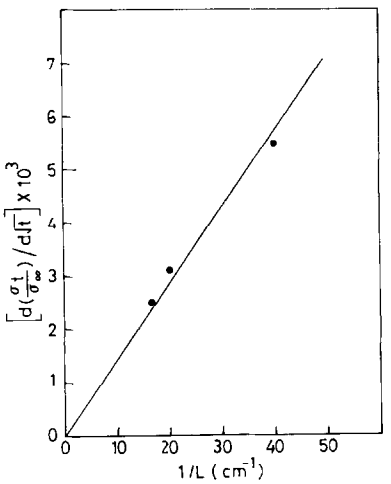

FIG. 6. The relation between the slopes of the linear plots of ln σ_t/σ_∞ vs $\sqrt{t}$ and $1/L$; the data are taken from region II in Fig. 1.

The important single parameter in Eq. (12) is the dimensionless group (Dt/L^2). Thus for a certain value of $\tau = Dt/L^2$, σ_t/σ_∞ has a unique value independent of the values of D, t, and L^2 of the system. Conversely, the time needed to reach a certain value of σ_t/σ_∞ for pellets of different thicknesses is directly proportional to L^2; i.e., t/L^2 is constant. Table I lists the values of $t_{(x)}/L^2$ for pellets of different thicknesses at three values of σ_t/σ_∞, as taken from Fig. 1. The constancy of these values confirms the validity of Eq. (12). Consequently, it is concluded that region III in Fig. 1 displays the behavior of the system under diffusion control.

References

1. J. BESSIERS, A. BESSIERES, AND J. J. HEIZMANN, *Int. J. Hydrogen Energy* **5**, 585 (1980).
2. N. RANACHANDRAN AND D. K. CHAKRABRTY, *Proc. Indian Acad. Sci. Chem. Sci.* **89**, 533 (1980).
3. J. BESSIERES, A. BESSIERES, AND J. J. HEIZMANN, *Hydrogen Energy Syst.* **4**, 1731 (1979).
4. M. M. KHADER, G. H. VURENS, I. K. KIM, M. SALMERON, AND G. A. SOMORJAI, *J. Am. Chem. Soc.* **109**, 358 (1987).
5. M. M. KHADER, N. N. LICHTIN, G. H. VURENS, M. SALMERON, AND G. A. SOMORJAI, *Langmuir* **3**, 303 (1987).

6. E. POLLERT, J. HEJTMANLK, J. P. DOUMERC, J. C. LAUNAN, AND P. HAGEMMULLER, *Z. Anorg. Allg. Chem.* **528,** 202 (1985).
7. A. H. A. TINNEMAN, T. P. M. KOSTER, AND A. MACKOR, *Ber. Bunsen-Ges. Phys. Chem.* **90,** 390 (1986).
8. P. MERCHANT, R. COLLINS, R. KERSHAW, K. DWIGHT, AND A. WOLD, *J. Solid State Chem.* **27,** 304 (1979).
9. R. F. G. GARDNER, F. SWEETT, AND D. W. TANNER, *J. Phys. Chem. Solids* **24,** 1175, 1183 (1963).
10. M. HENDEWERK, M. SALMERON, AND G. A. SOMORJAI, *Surf. Sci.* **172,** 544 (1986).
11. J. B. GOODENOUGH, "Progress in Solid State Chemistry" Reiss, Ed.) Vol. 5, p. 145, Pergamon, Oxford (1971).
12. FRANK WILKINSON, "Chemical Kinetics and Reaction Mechanisms," p. 28, Van Nostrand, New York (1980).
13. W. M. MCKEWAN, *Trans. Met. Soc. AIME* **224,** 387 (1962).
14. J. CRANK, *in* "The Mathematics of Diffusion," 2nd ed., pp. 47, 64, Clarendon Press, Oxford (1975).